

Supporting Information for

Synthesis of $[Fe(L)(bipy)]_n$ Spin Crossover Nanoparticles using Blockcopolymer Micelles.

Ottokar Klimm,^[a] Christoph Göbel,^[a] Florian Puchtler,^[c] Nobuyoshi Miyajima,^[d] Katharina Marquardt,^[d] Josef Breu,^[c] Sabine Rosenfeldt,^[b] Markus Drechsler,^[e] Stephan Förster,^[b] Birgit Weber^{[a]*}

^[a] Anorganische Chemie II, Universität Bayreuth, Universitätsstraße 30, NW I, 95440 Bayreuth, Germany, E-mail: weber@uni-bayreuth.de, <http://www.ac2-weber.uni-bayreuth.de>

^[b] Physikalische Chemie I, Universität Bayreuth, Universitätsstraße 30, NW I, 95440 Bayreuth, Germany

^[c] Anorganische Chemie I, Universität Bayreuth, Universitätsstraße 30, NW I, 95440 Bayreuth, Germany

^[d] Bayerisches Geoinstitut, Universität Bayreuth, Universitätsstr. 30, 95440 Bayreuth, Germany

^[e] Soft Matter Electron Microscopy, BIMF, Universität Bayreuth, Universitätsstraße 30, NW I, 95440 Bayreuth, Germany

Optimization of the reaction conditions

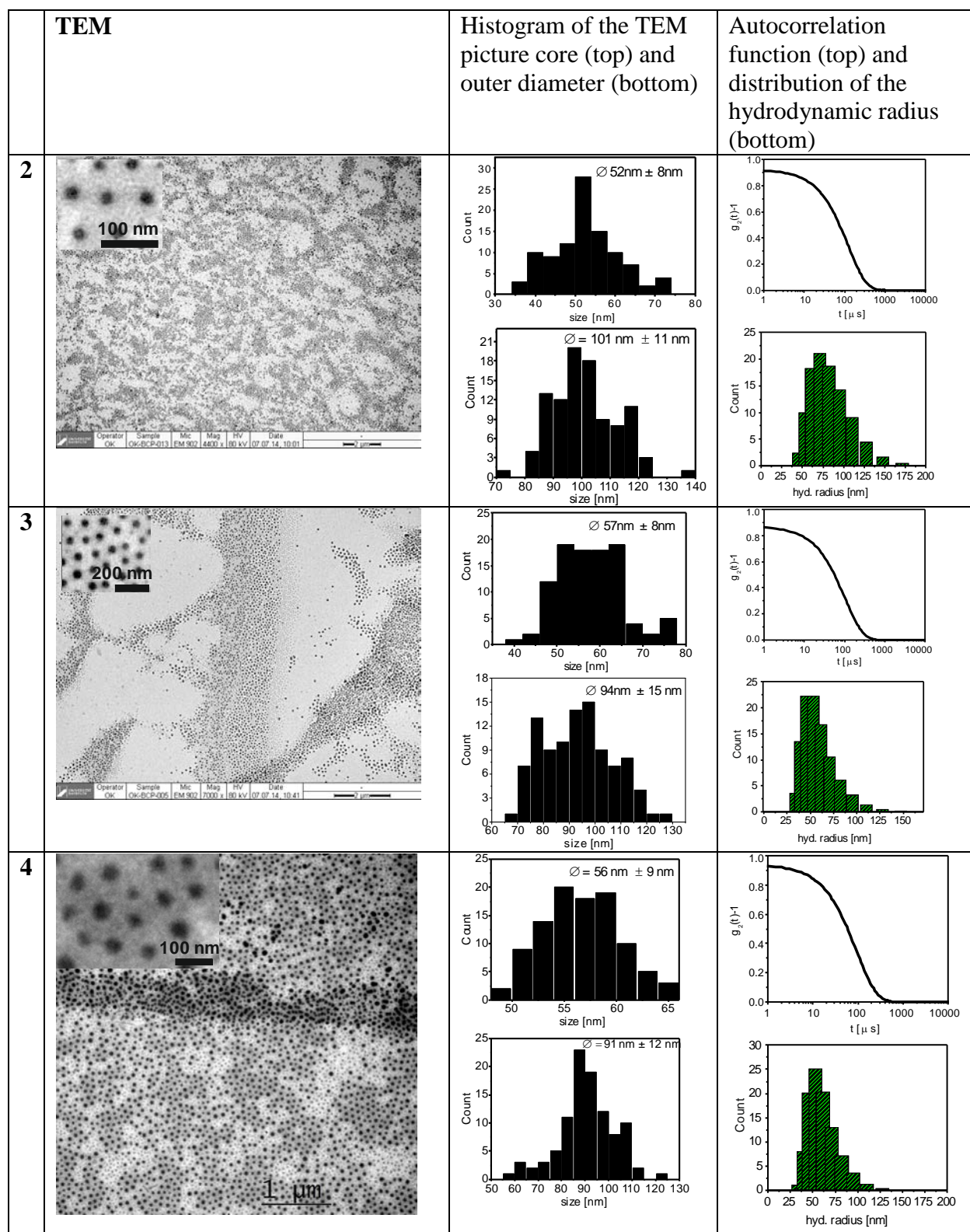
Synthesis of the CP-BCP samples 7-24:

PS-P4VP (50 mg, 0.33 µmol), [Fe(L)(MeOH)₂] (amount given in the Table) and THF (20 ml) were mixed and heated to reflux for 2h. After cooling to room temperature 4,4'-bipyridine (amount given in the Table) was added to the brown solution and the reaction mixture was heated for 1h (all samples except 16-20) or 15 min (16-20) to reflux. After cooling to room temperature the reaction was continued as given in the following overview using the same procedure as for the samples 2-6 for the different number of cycles. The results are summarized in Table S2.

Sample	cycles	Total reaction time	Reaction temperature	Amount of [Fe(L)(MeOH)₂] and bipy per cycle
7	1	3 h	66°C	[Fe(L)(MeOH) ₂]: 6.4 mg, 15 µmol bipy: 2.3 mg, 15 µmol
8	1	3 h	66°C	[Fe(L)(MeOH) ₂]: 6.4 mg, 15 µmol bipy: 6.8 mg, 45 µmol
9	1	3 h	66°C	[Fe(L)(MeOH) ₂]: 6.4 mg, 15 µmol bipy: 9.1 mg, 60 µmol
10	1	3 h	66°C	[Fe(L)(MeOH) ₂]: 6.4 mg, 15 µmol bipy: 11.3 mg, 75 µmol
11	3	5 h	66°C	[Fe(L)(MeOH) ₂]: 6.4 mg, 15 µmol bipy: 13.8 mg, 88 µmol
12	3	5 h	66°C	[Fe(L)(MeOH) ₂]: 6.4 mg, 15 µmol bipy: 15.7 mg, 101 µmol
13	3	5 h	66°C	[Fe(L)(MeOH) ₂]: 6.4 mg, 15 µmol bipy: 17.9 mg, 115 µmol
14	3	5 h	66°C	[Fe(L)(MeOH) ₂]: 6.4 mg, 15 µmol bipy: 20.2 mg, 129 µmol
15	3	5 h	66°C	[Fe(L)(MeOH) ₂]: 6.4 mg, 15 µmol bipy: 22.4 mg, 144 µmol
16	1	2.25 h	66°C	[Fe(L)(MeOH) ₂]: 6.4 mg, 15 µmol bipy: 5.6 mg, 36 µmol

17	2	2.5 h	66°C	[Fe(L)(MeOH) ₂]: 6.4 mg, 15 µmol bipy: 5.6 mg, 36 µmol
18	3	2.75 h	66°C	[Fe(L)(MeOH) ₂]: 6.4 mg, 15 µmol bipy: 5.6 mg, 36 µmol
19	4	3 h	66°C	[Fe(L)(MeOH) ₂]: 6.4 mg, 15 µmol bipy: 5.6 mg, 36 µmol
20	5	3.25 h	66°C	[Fe(L)(MeOH) ₂]: 6.4 mg, 15 µmol bipy: 5.6 mg, 36 µmol
21	1	3 h	RT	[Fe(L)(MeOH) ₂]: 6.4 mg, 15 µmol bipy: 5.6 mg, 36 µmol
22	2	4 h	RT	[Fe(L)(MeOH) ₂]: 6.4 mg, 15 µmol bipy: 5.6 mg, 36 µmol
23	3	5 h	RT	[Fe(L)(MeOH) ₂]: 6.4 mg, 15 µmol bipy: 5.6 mg, 36 µmol
24	5	7 h	RT	[Fe(L)(MeOH) ₂]: 6.4 mg, 15 µmol bipy: 5.6 mg, 36 µmol

Table S1. Characterization of the CP-BCP composite materials (samples 2–5). The results of TEM and DLS are summarized and discussed in the main text. Each sample was prepared at least twice.



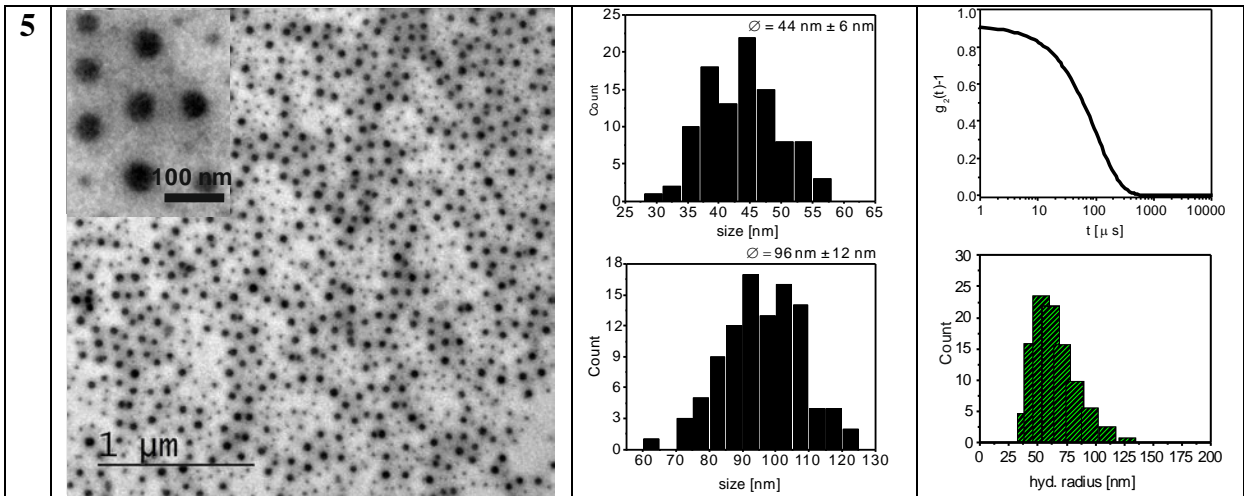
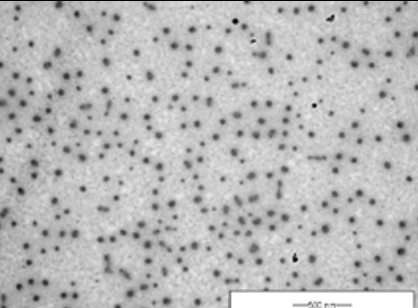
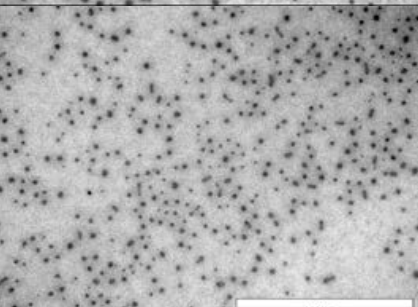
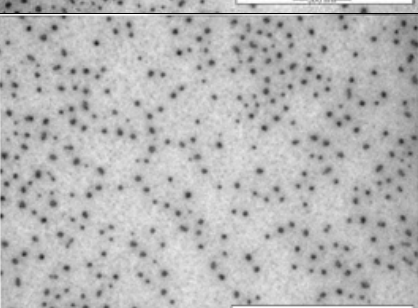
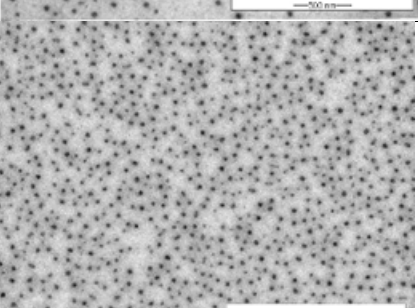
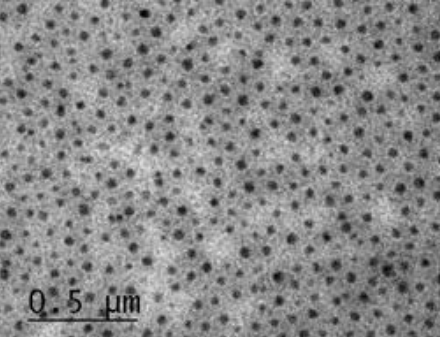
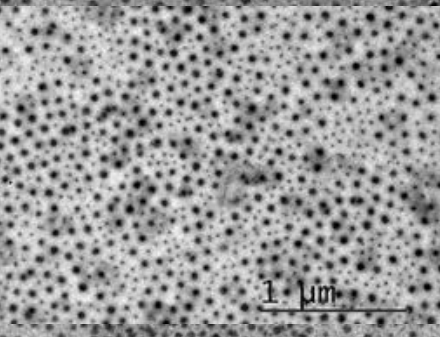
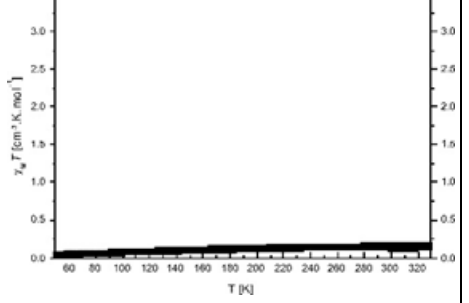
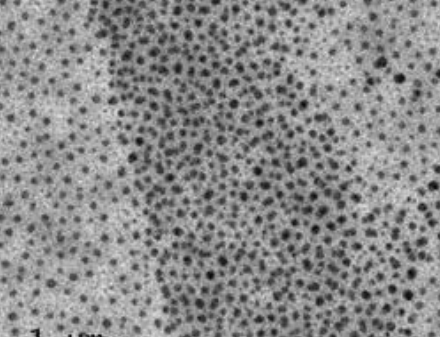
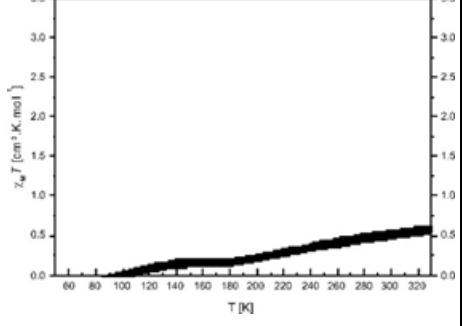
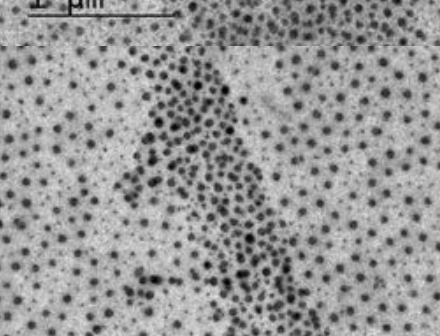
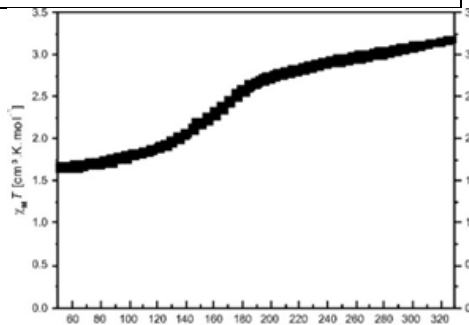
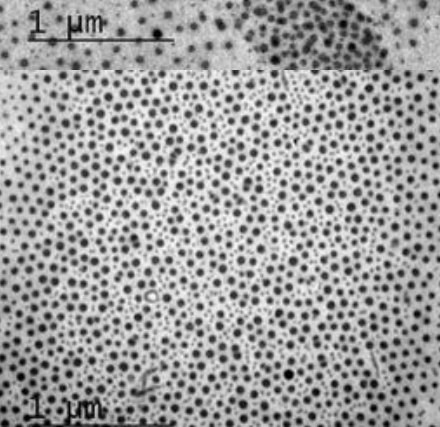
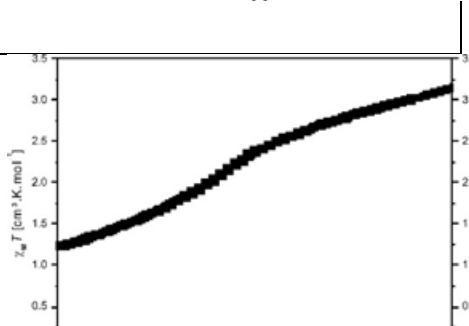
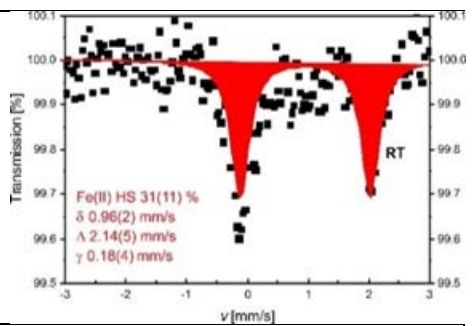
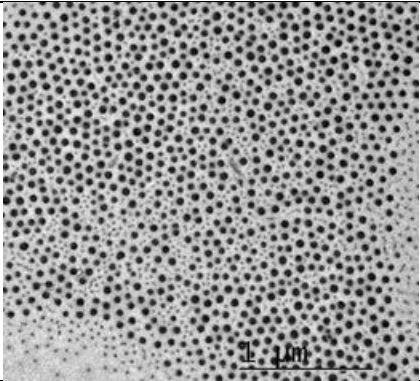
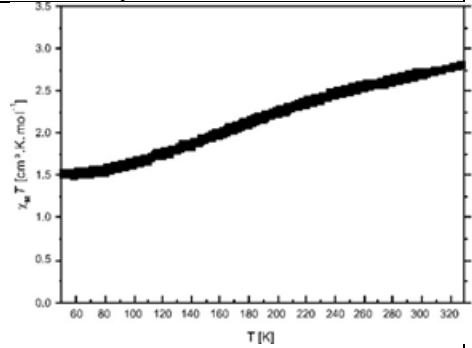
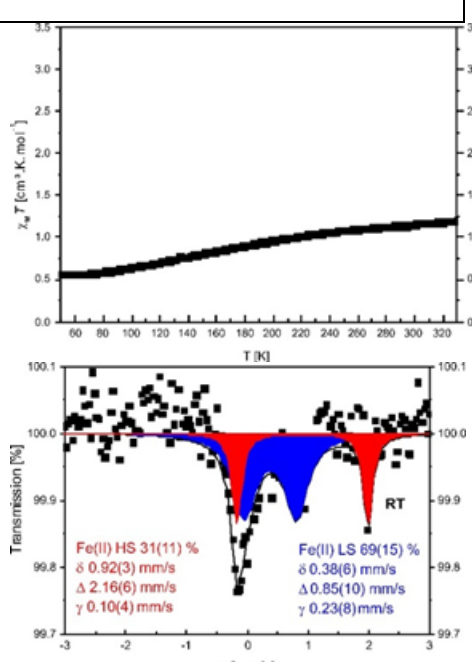
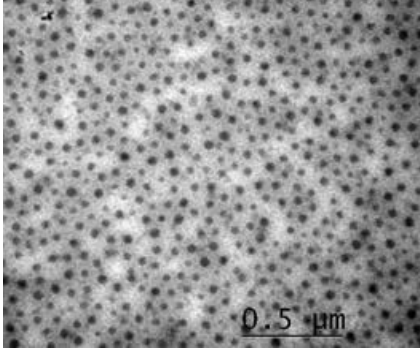
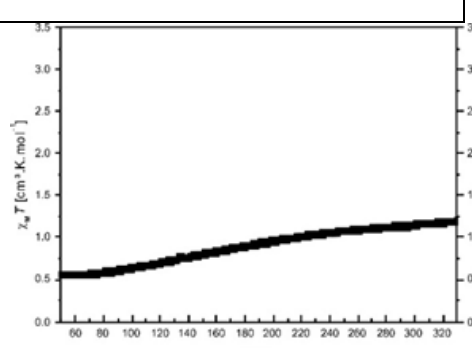
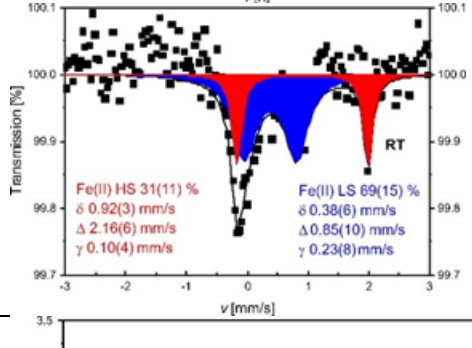
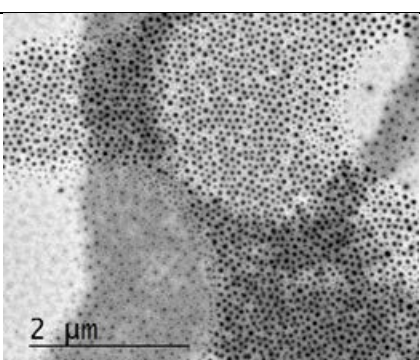
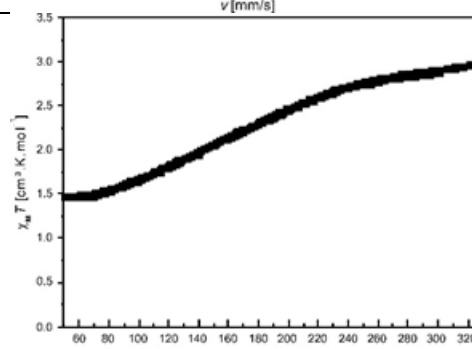
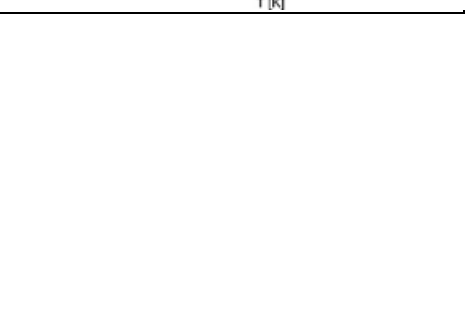
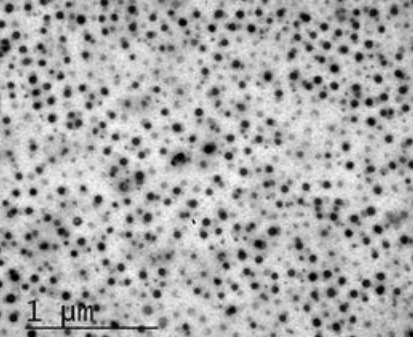
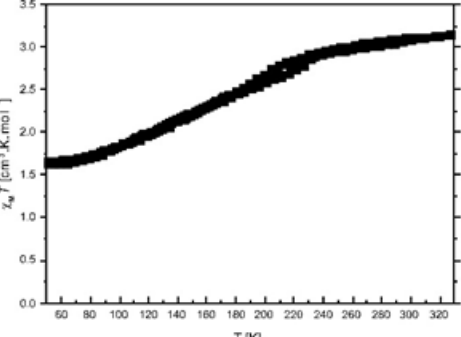
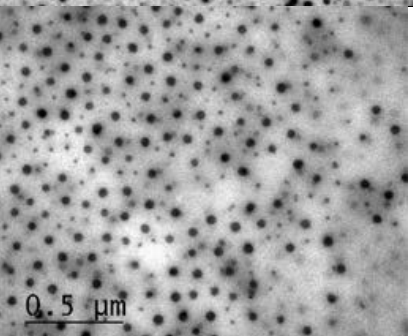
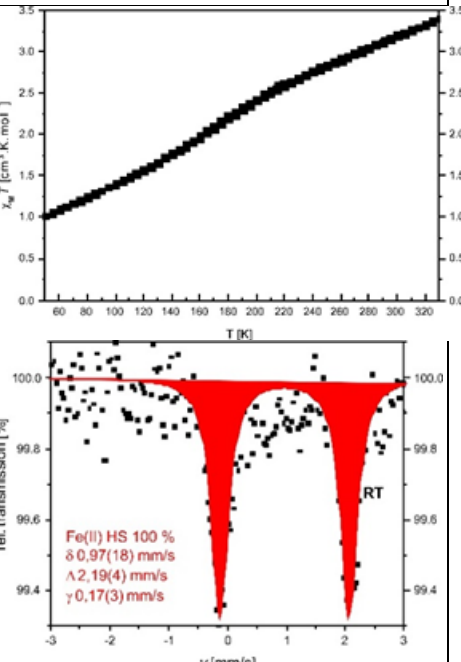
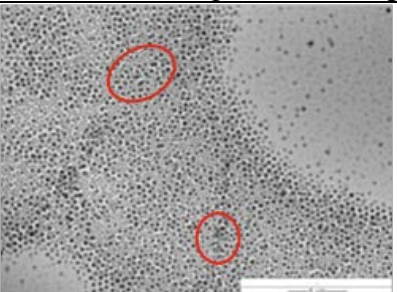
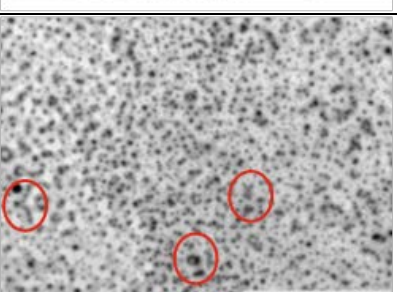


Table S2. Overview over the samples used for the determination of the optimum reaction conditions together with their TEM pictures and the results of SQUID measurements and Mössbauer Spectroscopy (if applicable). Red circles in the TEM pictures highlight significant parts.

Sample ([Fe(L]):bipy ; cycles; temperature; time)	TEM	core Size DLS/ TEM (core)	Magnetism / Mössbauer
Variation of the Fe:bipy ratio between 1:1 to 1:10 (samples 12 – 21)			
7 (1:1; 1; 66°C; 3h)		TEM: 43 ± 6 nm	
8 (1:3; 1; 66°C; 3h)		TEM: 40 ± 7 nm	
9 (1:4; 1; 66°C; 3h)		TEM: 50 ± 9 nm	
10 (1:5; 1; 66°C; 3h)		TEM: 51 ± 8 nm	

15 (1:10; 3; 66°C; 5h)		DLS: 140 nm TEM: 36 ± 6 nm	
14 (1:9; 3; 66°C; 5h)		DLS: 130 nm TEM: 43 ± 7 nm	
13 (1:8; 3; 66°C; 5h)		TEM: 47 ± 7 nm	
12 (1:7; 3; 66°C; 5h)		TEM: 50 ± 8 nm	
11 (1:6; 3; 66°C; 5h)		TEM: 43 ± 4 nm	

			
Reduction of the reaction time to 15 min (1 – 5 cycles)			
16 (1:2.5; 1; 66°C; 2.25h)		DLS: 138 nm TEM: 52±5 nm	 
17 (1:2.5; 2; 66°C; 2.5 h)		DLS: 146 nm TEM: 51±6 nm	 
18 (1:2.5; 3; 66°C; 2.75 h)		DLS: 146 nm TEM: 51±10 nm	 

19 (1:2,5; 4; 66°C; 3 h)		DLS: 147 nm TEM: 53±5 nm	
20 (2:2,5; 5; 66°C; 3.25 h)		TEM: 42±5 nm	
Stirring at room temperature (1 – 5 cycles)			
21 (1:2,5; 1; RT; 3h)		TEM: 56±7 nm	
22 (1:2,5; 2; RT; 4h)		TEM: 35±6 nm	

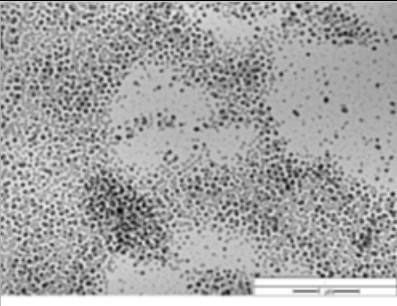
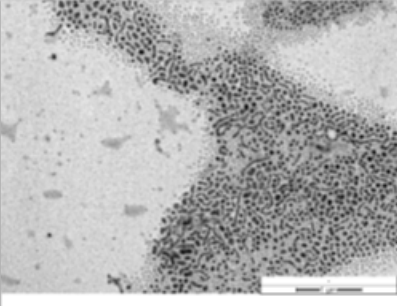
23 (1:2.5; 3; RT; 5h)		TEM: 58 ± 9 nm	
24 (1:2.5; 5; RT; 7h)		TEM: 63 ± 13 nm	

Table S3. Mössbauer parameters of the samples **1** and **3 – 6** at room temperature. Given are the isomer shift δ [mm s⁻¹], the quadrupole splitting ΔE_Q [mm s⁻¹], the half width of the lines Γ [mm s⁻¹], and the fraction of HS sites [%].

compound	Site	δ [mm·s ⁻¹]	ΔE_Q [mm·s ⁻¹]	Γ [mm·s ⁻¹]	A/A _{tot} [%]
1	Fe ^{II} LS	0.38(4)	0.69(3)	0.22(3)	81(6)
	Fe ^{II} HS	0.96(3)	2.23(3)	0.32(2)	19(7)
3	Fe ^{II} LS	0.38(4)	1.01(8)	0.38(4)	47(4)
	Fe ^{II} HS	0.96(3)	2.21(6)	0.32(3)	53(4)
4	Fe ^{II} LS	0.45(9)	0.84(16)	0.49(12)	45(15)
	Fe ^{II} HS	0.93(2)	2.20(4)	0.24(6)	55(12)
5	Fe ^{II} LS	0.28(4)	1.02(8)	0.22(12)	16(6)
	Fe ^{II} HS	0.97(13)	2.15(3)	0.32(4)	84(8)
6	Fe ^{II} LS	-	-	-	-
	Fe ^{II} HS	0.95(5)	2.17(1)	0.28(2)	100

Figure S1. Left: TEM picture of the empty PS-P4VP BCP. Middle: Results of dynamic light scattering of the PS-P4VP-BCP in THF showing a hydrodynamic diameter of 126 nm. Right: size histogram from the TEM picture given on the left with an average diameter of 70 nm.

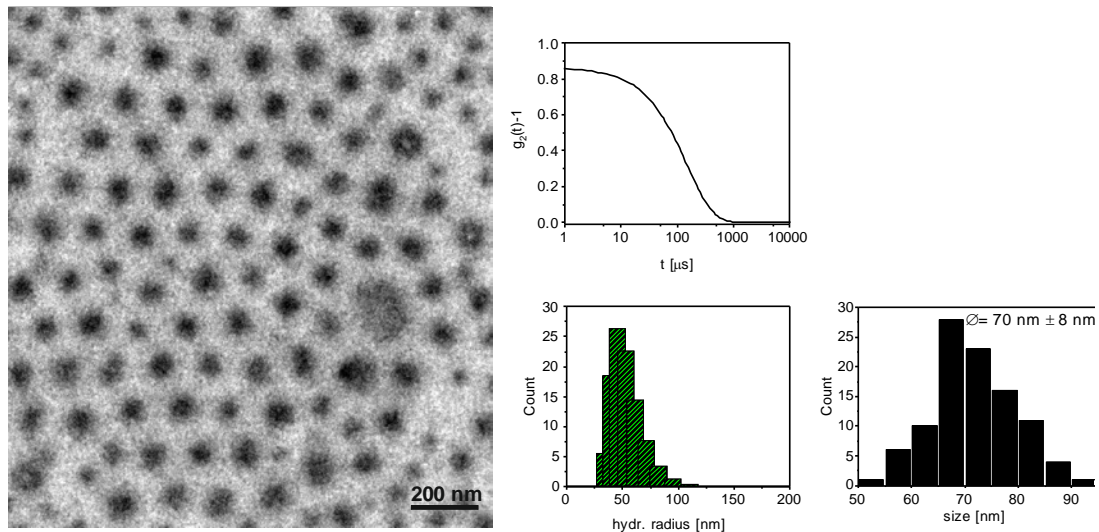


Figure S2. Mössbauer spectrum of **1** at room temperature. Two doublets are observed corresponding to two different species $[\text{Fe}(\text{L})(\text{vp})]$ and $[\text{Fe}(\text{L})(\text{vp})_2]$. The majority species (blue doublet, 80 %) with an isomer shift δ of $0.38(4)$ mm/s and a quadrupole splitting ΔE_Q of $0.69(3)$ mm/s corresponds to an octahedral LS complex $[\text{Fe}(\text{L})(\text{vp})_2]$, while the parameters of the minority species (red doublet, 20 %, $\delta = 0.96(3)$ mm/s and $\Delta E_Q = 2.25(9)$ mm/s) is characteristic for an HS complex $[\text{Fe}(\text{L})(\text{vp})]$.

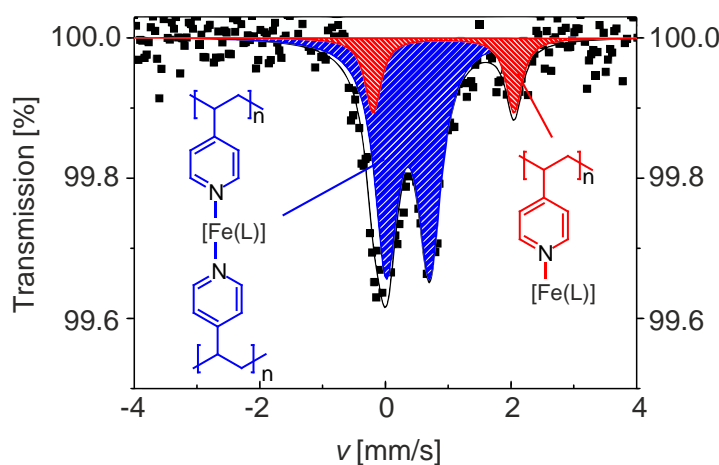


Figure S3. IR spectra of the BCP, $[\text{Fe}(\text{L})(\text{bipy})]_n$ and the composite samples **2 – 6**.

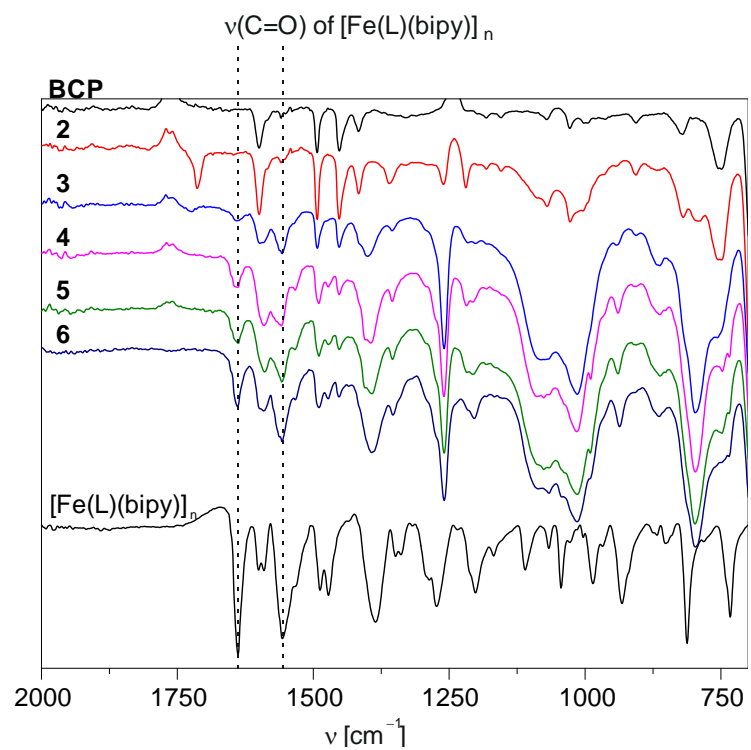
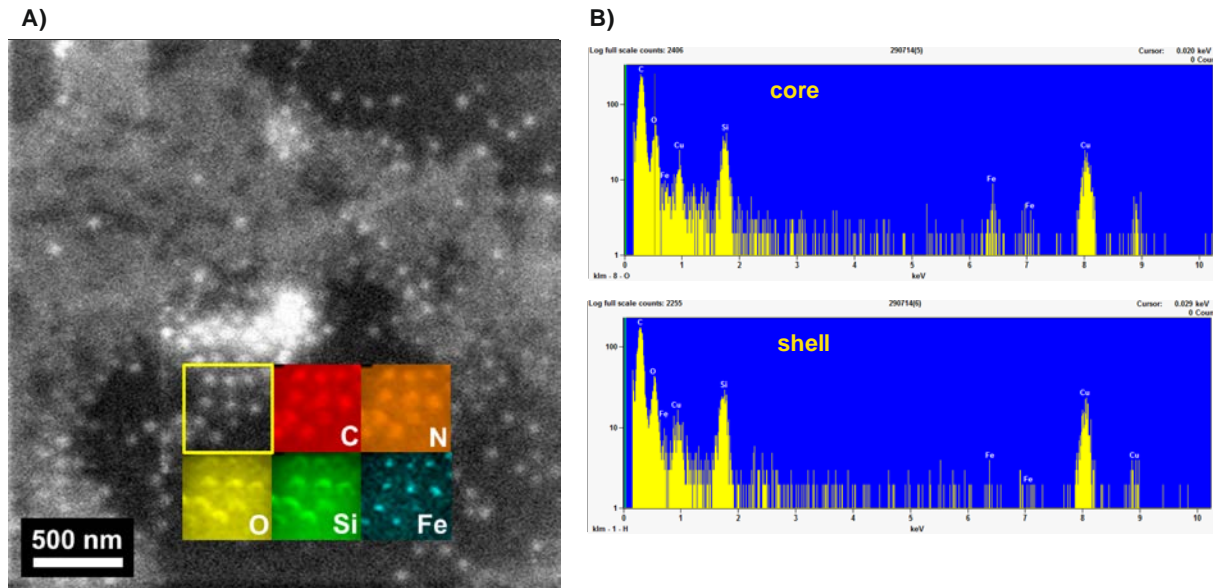
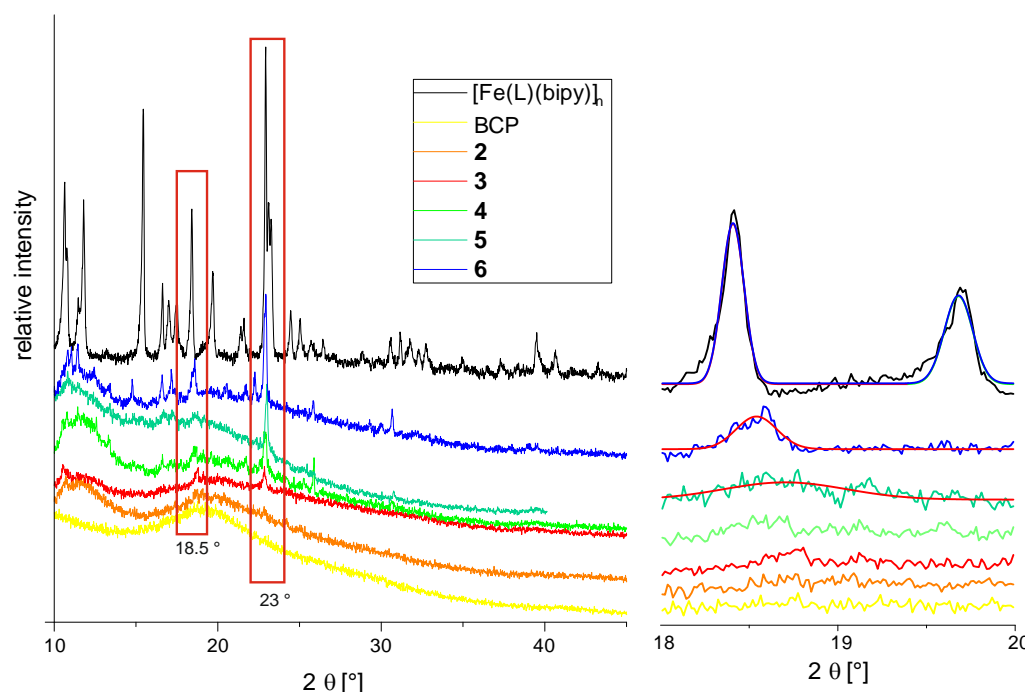


Figure S4. A) 2D-EDX screening of CP-BCP micelles of sample **6** to show the distribution of iron (blue), carbon (red), nitrogen (orange), oxygen (yellow) and silicon (green) in the sample. A significant difference is observed for the iron distribution in the core (bright, high amount of iron) and the shell (dark, low amount of iron). B) EDX analysis of the core and the shell of the CP-BCP micelle showing a significant difference in the iron distribution.



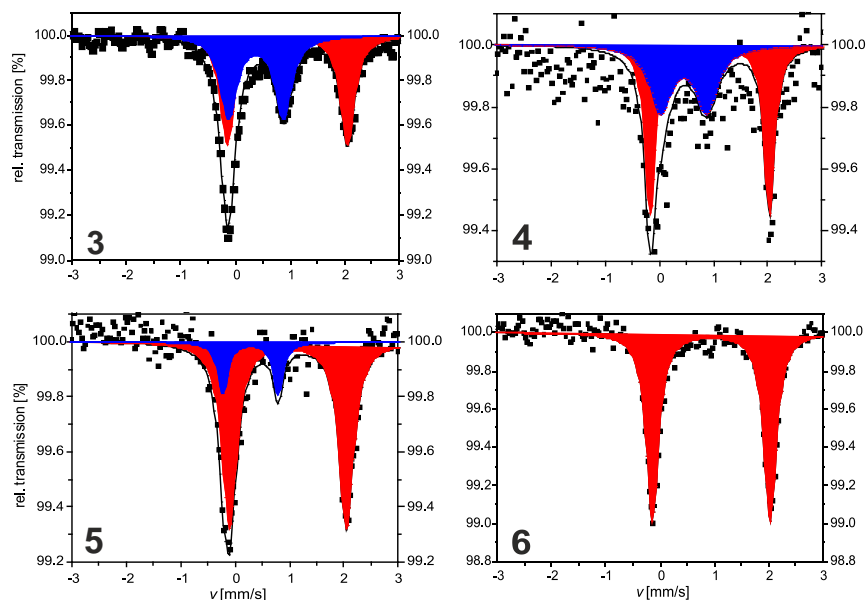
As shown in Figure S4A the spherical core of the NPs (bright spot) shows mainly the elements carbon, iron and nitrogen. In contrast to this, there is almost no iron in the outer shell, while carbon and nitrogen are evenly distributed over the whole particle. The EDX analysis (Fig. S4B) is given for the core (top) and the outer shell (bottom) of the NPs. It also confirms that the core of the NP has a significant amount of iron while the shell is nearly iron-free. The copper signal in both measurements arises from the TEM grids and the silicon most likely from the synthesis of the CP-BCP composite materials (small amount of grease).

Figure S5. PXRD spectra in the $10 - 45$ 2θ range of the samples **2 – 6**, the bulk complex $[\text{Fe}(\text{L})(\text{bipy})]_n$ and the BCP. The peaks used for the calculation of the particle size are indicated with red squares. For the complex $[\text{Fe}(\text{L})(\text{bipy})]_n$ a good agreement between the particle size calculated from the two different peaks is observed (in both cases around 60 nm). For the composite material the particle sizes determined from the 18.5° peak are smaller (10 nm for **5** and 30 nm for **6**) compared to the values obtained for the 23° peak discussed in the manuscript. The continuous line resembles the fit used for the determination of the half width.



To analyze the crystallinity of the obtained particles, powder X-ray diffraction data were collected for the different samples. After one cycle (sample **2**), no reflexes are observed indicating a completely amorphous material. With increasing number of cycles, some broad reflexes appear in a similar region as for the bulk $[\text{Fe}(\text{L})(\text{bipy})]_n$. Those reflexes are significantly broader and less well defined than those reported for microcrystals of $[\text{Fe}(\text{L})(\text{bipy})]_n$ in a P4VP matrix.¹ Even after 5 cycles (sample **6**), the typical PXRD pattern of the bulk material is not observed – some reflexes are missing. This indicates that the crystalline parts of the particles are much smaller than those obtained in the P4VP matrix.

Figure S6. Room temperature Mössbauer spectra of the samples **3 – 6**. The black squares are the results from the measurements and the solid lines correspond to the fit with the low-spin doublet given in blue and the high-spin doublet given in red for each sample. The corresponding Mössbauer parameters are summarized in Table S4.



For all spectra, the signal intensity is comparatively low (around 1 % absorption) and the half width of the lines (Γ) is between 0.2 and 0.5 mm/s. This is significantly broader than the values observed for the sub-microcrystals of $[\text{Fe}(\text{L})(\text{bipy})]$ in the P4VP matrix.¹ Both observations are typical for nanoparticles. For the iron complex $[\text{FeL}]$ in the polymer matrix before addition of the bridging ligand bipy (sample **1**, in Figure S2) two doublets are observed. The main species with an area of 81(6) % shows Mössbauer parameters ($\delta = 0.38(4)$ mm/s, $\Delta E_Q = 0.69(3)$ mm/s) typical for octahedral iron(II) LS sites of this ligand type.^{2,3} This corresponds to a complex with two vinylpyridine units coordinating at the iron center. The second doublet ($\delta = 0.96(3)$ mm/s, $\Delta E_Q = 2.23(3)$ mm/s) shows typical parameter for iron(II) HS complexes of this ligand type.^{2,3} This HS site with an area of 19(7) % corresponds to an iron(II) species with one vinylpyridine coordinated to the iron center leaving the sixth coordination site free or occupied by one solvent molecule. Iron(II)

complexes of this ligand type with an N₃O₂ or an N₃O₃ coordination sphere are usually in the HS state.^{4–6} Upon addition of bipy, the desired coordination polymer is formed. Magnetic measurements on the bulk material revealed an abrupt and complete spin transition with hysteresis (18K, $T_{1/2\downarrow} = 219\text{K}$ and $T_{1/2\uparrow} = 237\text{K}$) below room temperature,^{7–9} thus at room temperature the complex is in the HS state. In agreement with this, upon addition of bipy the area of the LS doublet decreases and the area of the HS doublet increases. The Mössbauer parameters of the HS state do not change significantly upon coordination of the pyridine and are in the same range as observed for the bulk material and sub-microcrystals of [Fe(L)(bipy)] in P4VP.¹ When going from **3** to **6**, with an increasing number of reaction cycles, the area fraction of the LS species continuously decreases until for sample **6** only one HS doublet is observed (see Table 3).

References

1. Göbel, C.; Palamarciuc, T.; Lochenie, C.; Weber, B. *Chem. Asian J.* **2014**, 9 (8), 2232–2238.
2. Bauer, W.; Lochenie, C.; Weber, B. *Dalton Trans.* **2014**, 43 (5), 1990–1999.
3. C. Lochenie, C.; Bauer, W.; Railliet, A. P.; Schlamp, S.; Garcia, Y.; Weber, B. *Inorg. Chem.* **2014**, 53 (21), 11563–11572.
4. Weber, B.; Kaps, E.; Obel, J.; Bauer, W. Z. *Anorg. Allg. Chem.* **2008**, 634 (8), 1421–1426.
5. Bauer, W.; Weber, B. *Acta Cryst. C* **2008**, 64 (6), m237.
6. Weber, B.; Jäger, E.-G. *Eur. J. Inorg. Chem.* **2009**, 2009 (4), 465–477.
7. Weber, B.; Tandon, R.; Himsl, D. Z. *Anorg. Allg. Chem.* **2007**, 633 (8), 1159–1162.
8. Weber, B.; Kaps, E. S.; Desplanches, C.; Létard, J. *Eur. J. Inorg. Chem.* **2008**, 2008 (19), 2963–2966.
9. Baldé, C.; Bauer, W.; Kaps, E.; Neville, S.; Desplanches, C.; Chastanet, G.; Weber, B.; Létard, J. F. *Eur. J. Inorg. Chem.* **2013**, 2013 (15), 2744–2750.